coatings

MDPI

Article

Chitosan Coating Loaded with Spearmint Essential Oil Nanoemulsion for Antifungal Protection in Soft Citrus (*Citrus reticulata*) Fruits

Lebogang T. C. Maswanganye [1], Sreejarani Kesavan Pillai [1,2] and Dharini Sivakumar [1,3,*]

[1] Phytochemical Food Network Group, Department of Crop Sciences, Tshwane University of Technology, Pretoria West, Pretoria 0001, South Africa; lebogangbatista@gmail.com (L.T.C.M.); skpillai@csir.co.za (S.K.P.)
[2] Centre for Nanostructures and Advanced Materials, DSI/CSIR Nanotechnology Innovation Centre, Council for Scientific and Industrial Research, Pretoria 0001, South Africa
[3] Centre for Nutrition & Food Sciences, Queensland Alliance for Agriculture and Food Innovation, The University of Queensland, Brisbane, QLD 4108, Australia
* Correspondence: sivakumard@tut.ac.za or d.sivakumar@uq.edu.au

Abstract: In this study, chitosan (CH) was loaded with spearmint (S) essential oil nanoemulsion (EO) to provide antifungal properties during the postharvest storage of soft citrus fruits. (S)-EO (2%) nanoemulsion–CH (0.8%) coatings inhibited 100% of *Penicillium italicum* and *Penicillium digitatum* radial mycelial growth and spore germination in vitro. The (S)-EO (2%) nanoemulsion–CH coating (0.8%) enhanced the antifungal activity by achieving 100% inhibition of *P. digitatum* in soft citrus cultivars 'Nova' and 'Tango' compared to the control in vivo. However, *P. italicum* decay was reduced to 33% and 18% in 'Nova' and 'Tango' soft citrus compared to the control. The (S)-EO (2%)-CH nanoemulsion coating system prepared by high shear homogenization showed a particle size of 252.3 nm and zeta potential of +21.6 mV, indicating changes in molecular interactions and structural reorganization between EO and CH. The polydispersity index values indicated a stable system. pH remained acidic, antifungal activity was favored, and the incorporation of the EO nanoemulsion improved the thermal stability of the CH coating. The optical properties showed less transparency and more opacity. Despite cultivar differences affecting host specificity, the study recommends using a 2% (S)EO nanoemulsion–CH (0.8%) coating instead of synthetic chemicals to extend citrus fruit storage life.

Keywords: essential oil; nanoemulsion; edible coating; clementines

Academic Editor: María B. Pérez-Gago

Received: 29 November 2024
Revised: 11 January 2025
Accepted: 15 January 2025
Published: 18 January 2025

Citation: Maswanganye, L.T.C.; Pillai, S.K.; Sivakumar, D. Chitosan Coating Loaded with Spearmint Essential Oil Nanoemulsion for Antifungal Protection in Soft Citrus (*Citrus reticulata*) Fruits. *Coatings* **2025**, *15*, 105. https://doi.org/10.3390/coatings15010105

1. Introduction

Globally, citrus fruit has the highest economic value. Citrus consumption has been directly associated with a reduced risk of chronic illnesses, including cancer, cardiovascular diseases, and diabetes [1]. Citrus fruit consumption has increased due to consumer interest in nutrition and health benefits. In 2024, the global production of 'soft citrus' fruits known as 'easy peelers' was projected to rise by 4% to reach 33.3 million MT [2]. Soft citrus (*Citrus reticulata*) fruits include tangerines, clementines, satsumas, and mandarins. Significant economic loss occurs through green and blue molds caused by *Penicillium italicum* (blue mold decay) and *Penicillium digitatum* (green mold decay) during distribution and marketing [2]. The two pathogens infect fruit surfaces through wounds and have an extremely short shelf life (3–5 days at 25 °C) [3]. The use of Imazalil (IMZ) (dichlorophenethyl imidazole) (4), a widely used synthetic chemical for postharvest applications, was slated to end in 2021 [3]. By 2030, the European Green Deal aims for a 50% reduction in chemicals used in

agriculture, including more hazardous pesticides [4]. Thiabendazole, Imazalil, and sodium o-phenylphenate resistance are on the rise [3].

As a result, natural and sustainable ways to extend perishable items' shelf lives and safety are becoming increasingly popular. As a promising technology, antifungal edible coatings have the potential to reduce the need for synthetic preservatives while retaining the quality of fresh fruit [5]. Polymeric coatings based on polysaccharides are readily available, non-allergenic, water-soluble, and have good mechanical properties [6]. Polysaccharide coating chitosan (2-amino-2-deoxy-bD-glucosamine) (CH) made from shrimp and crab exoskeletons is low-cost and has Generally Recognized as Safe (GRAS) compliance [6]. However, seasonality and fishing restrictions have made it difficult to source shrimps for chitosan production [7]. Additionally, chitosan's quality is affected by metal contamination. *Hermetia illudens*, Diptera, Black soldier fly, is a non-pest fly that converts organic waste into nutrients [8]. These flies are good sources of chitin and chitosan with the same purity and chemical characteristics as commercially available polymers [7]. Their hydrophilicity, biodegradability and biocompatibility, film-forming, non-toxic, antimicrobial properties, and ability to combine with other biopolymers due to their amino group charge $(NH_3)^+$ have attracted food-related and industry attention [6]. Furthermore, CH films can carry antioxidants, flavoring compounds, and essential oils that enhance the antimicrobial properties of fruits and extend their shelf life [9]. Moreover, Chien et al. [10] showed that 0.1% Low-Molecular-Weight Chitosan (LMWC) coating dramatically reduced the decay of Murcott tangor held at 15 C compared to the control samples. Compared to TBZ, it reduced decay by over 20%. Citrus fruits were protected against *Penicillium digitatum* and *Penicillium italicum* proliferation by LMWC at a concentration of 0.2%.

Furthermore, Perdones et al. [11] demonstrated that the addition of lemon essential oil (3% (*w*/*w*) to chitosan (1%, *w*/*w*) increased the antifungal activity of chitosan both in vitro and in cold storage conditions in strawberries inoculated with spore suspensions of *Botrytis cinerea*. According to Sanchez-González et al. [12], films containing the maximum amount of bergamot oil (3:1 BO:CH ratio) were effective in the total inhibition of fungus growth within five days at 20 °C. Spearmint (S) essential oil (EO) can be incorporated into edible coatings to improve efficacy and decrease losses [13]. A widely consumed aromatic plant in the Lamiaceae family is spearmint (*Mentha spicata* L.). It has strong antifungal properties, making it a suitable candidate for controlling citrus postharvest pathogens [14]. Dihydrocarvone, dihydrocarveol, and carveol are the primary components of spearmint. Phala et al. [14] also reported that carvone has strong antifungal properties against major citrus postharvest pathogens. However, since citrus is shipped in open telescopic boxes, EO application in the vapor phase is impractical. As essential oils are well documented for their volatility, instability, and poor solubility, combining them with polymers has proved successful in overcoming these challenges [14]. Additionally, strong EO odors and tastes can also affect the sensory properties of fruit. Nanoemulsions of essential oils can minimize this problem. Made through a low-energy natural emulsification process, nanoemulsions have smaller droplets that have the potential to prevent microbial growth and preserve quality better during storage compared to larger droplets [15]. The inherent advantages of nanoemulsions, such as increased surface area and improved dispersibility, contribute to these beneficial effects on product quality maintenance [16].

As the studies demonstrating the effectiveness of nanoemulsion-based coatings of EOs are limited, it is crucial to evaluate the coating efficiency preservation performance of such encapsulated nanoemulsions to establish their successive consolidation into postharvest treatment strategies. Therefore, this study examined the antifungal properties of chitosan coatings containing different spearmint oil (S)-EO concentrations in soft citrus fruits. The four objectives of the current study were first, to test a spearmint oil nanoemulsion against

P. digitatum and *P. italicum* in vitro to determine their inhibition of radial mycelial growth and spore germination and second, to test the effect of the selected concentration of the (S)-EO nanoemulsion incorporated into selected CH coatings on the inhibition of the radial mycelial growth and spore germination of *P. digitatum* and *P. italicum* in vitro. The third objective investigated the rheological, physical, microstructural, and mechanical properties of the formulation of the (S)-EO nanoemulsion and CH. Lastly, in vivo tests of the formulation of spearmint oil and chitosan coating against *P. digitatum* and *P. italicum* were carried out for mold rot prevention.

2. Materials and Methods

2.1. Chemicals

Chitosan (CH) (CS, MW 50–190 kDa, deacetylation degree 75–85%, purity 75%) fungal growth medium and all chemicals were obtained from Sigma Aldrich (St. Louis, MO, USA). Spearmint (S) essential oil (EO) (*Mentha spicata*) was obtained from Holistic Emporium (Johannesburg, Gauteng, South Africa).

2.2. Fungal Cultures

Fruit and Vegetable Technology Laboratories, Tshwane University of Technology, South Africa, provided fungi cultures (*P. italicum* and *P. digitatum*). The DNA-sequenced original fungal cultures were obtained from Plant Health and Protection (ARC-PHP), Roodeplaat (West), Pretoria, South Africa. A potato dextrose agar (PDA) medium was used to maintain the fungal isolates for 12–13 days at 25 °C. To obtain a pure and distinct colony, fungal isolates were sub-cultured on PDA plates.

2.3. Preparation of (S)-EO Nanoemulsion and CH Solution

(S)-EO at concentrations of 0.5, 1, and 1.5% (*v*/*v*) were dispersed in distilled water with 0.5% tween 80 as the emulsifier and stirred for 30 min. High-speed homogenization was applied to the emulsion using the IKA® Ultraturax (Staufen, Germany) at 10,000 rpm for 10 min, followed by ultrasonication (450 W, 20 khz) (Skymen Ultrasonic JP 100S (Guangdong, China)) at 20 °C for 10 min [17]. The CH solution was prepared by dissolving 0.5, 0.8, and 1.0 g of CH separately in 100 mL of purified water containing 0.5 mL (*v*/*v*) of acetic acid. Continuous stirring was performed throughout 24 h of heating, and 1 N NaOH was added to maintain a pH of 5.6 [9]. The pH was retained at 5.6 since the solubility of chitosan is attributed to the protonation of its amino groups in acidic solutions with a pH below 6.5 according to Badawy and Rabea [18].

2.4. In Vitro Antifungal Assay

The effectiveness of the CH solution and (S)-EO nanoemulsions for the inhibition of the radial mycelial growth of two citrus fruit decay fungi was evaluated individually using the poison food technique. First, 5 mm diameter agar disks from pure cultures of *P. digitatum* and *P. italicum* were placed at the center of a PDA dish containing an (S)-EO nanoemulsion at concentrations of 0.5%, 1.0%, and 1.5% and CH alone at concentrations of 0.2%, 0.4%, 0.8%, and 1.0%. For the coating systems, the (S)-EO nanoemulsion in combination with different CH concentrations was tested to determine its efficacy, and the optimal combination was selected to prepare the coating film. Control dishes contained only PDA or Imazalil fungicide treatment. The Petri dishes were then incubated at 25 °C for 7 days, with the radial growth of the fungus being measured every day until it reached the margins of the control dish. Vernier calipers (Digimatic, Mitutoyo Co., Ltd., Kanagawa, Japan) were used to measure colony diameter. Using the formula below [6], antifungal activity was expressed as a percentage of Inhibition of Mycelia Growth (IMG).

$$\text{Inhibition of Mycelia Growth } (\%) = \frac{\text{dc} - \text{dt}}{\text{dc}} \times 100$$

where dc = average diameter of control plate; dt = average diameter of treated plate.

Furthermore, antifungal minimum inhibitory concentrations (MICs) are the lowest concentrations of antifungal agents that are effective in preventing microorganisms from growing visibly for a set period [19]. MICs play a key role in determining an organism's susceptibility to antifungal agents [19].

The mycelial plugs that showed no growth were transferred to freshly poured PDA plates to determine the fungicidal or fungistatic activity of the (S)-EO nanoemulsion or CH coating. After 7 days at 25 °C, they were incubated to observe growth recovery. A fungicidal effect is indicated by no growth, while a fungistatic effect is indicated by growth [20].

Inhibition of spore germination: The efficacy of the (S)-EO nanoemulsions in inhibiting spore germination was determined according to Sivakumar et al. [21]. The spore suspensions were filtered with cheesecloth to detach the spores from the mycelium and fragments of the solid PDA medium, and then, the spore concentrations were adjusted with sterile distilled water to 10^6 spores/ mL. To evaluate the effect of treatments on spore germination, the prepared spore suspensions of *P. italicum* and *P. digitatum* were added to liquid potato dextrose broth (v/v) amended with different concentrations of the treatments. Cultures were incubated for 24 h at 28 °C. This experiment was repeated twice over time with three replicates. After the incubation period, the germination of 200 spores per plate was assessed under a microscope (Axiophot Carl Zeiss, Jena, Germany) at 100× magnification. When a conidium's germ tube exceeded half its length, it was considered germinated. Sterile distilled water (0.1 mL) and Imazalil (250 mg/L) treatments served as the control.

Each treatment was replicated three times. The inhibition rate (%) of the spore germination of isolated fungus was determined using the following formula:

$$\%\text{Inhibition of Spore Germination } (\%) = \frac{\text{N1} - \text{N2}}{\text{N1}}$$

N_1: Average number of spores germinated in the absence of treatments.
N_2: Average number of spores germinated in the presence of treatments. The IC_{50} values (concentration that resulted in 50% inhibition of germination) were estimated from data on spore germination and derived from nonlinear regression models [22].

2.5. Preparation of (S)-EO Nanoemulsion–CH Coating Solution and Films

Using radial mycelial growth assays, CH coating and (S)-EO nanoemulsion concentrations were selected for the fabrication of spearmint EO nanoemulsion–CH coatings. The (S)-EO nanoemulsion–CH coating was prepared by progressively dissolving CH (0.8%, w/v) firstly in ultrapure water (50 °C) with glacial acetic acid (0.5%, w/v) under constant stirring for 1 h. Glycerol was added to the above-prepared CH solution at a concentration of 40 wt%. A 2% (S)-EO nanoemulsion containing 1.5% (S)-EO (optimum based on in vitro antifungal assay) was mixed with the CH solution with a homogenizer (D-500 High Shear Homogenizer, H-600 Stand, DS-500/1 Shaft, Forrestdale, WA, USA) for 5 min at 10,000 rpm. A CH solution without an (S)-EO nanoemulsion served as the reference. The films from the corresponding solutions were prepared by the film casting method [23]. The coating formulations were poured onto a series of Petri dishes in the same quantity to give a final film thickness of 70 ± 5 µm. The film-forming suspensions were dried at 25 ± 2 °C and 50 ± 1% RH in a ventilated chamber (KBF 720 Binder, Tuttlingen, Germany) for 24 h. Then, the films were peeled off and conditioned again at 50 ± 1% RH and 25 ± 2 °C for 48 h before testing.

2.6. Characterization of Coating Formulation and Film

2.6.1. Particle Size, Polydispersity Index (PDI), Zeta Potential

The polydispersity index (PDI) analysis, zeta potential, and particle size of the (S)-EO nanoemulsion–CH coating solutions were determined according to Galus and Kadzińska [23] using dynamic light scattering (DLS) using a Zetasizer (Malvern Zetasizer Nanosizer®, Malvern Instruments Ltd., Worcestershire, UK) at a scattering angle of 90° and a temperature of 25 °C. To eliminate numerous scattering effects, samples were diluted with Milli-Q deionized water (1:10) before analysis [24]. All analyses were performed in triplicate and average values were reported.

2.6.2. Color and Transmittance of Coating Films

The film color was determined using a Konica® colorimeter (CR-10, Konica Minolta, Osaka, Japan). The white tile was used as standard during the color measurement. Lightness (L^*) and chromaticity parameters a^* (red-green) and b^* (yellow-blue) values were measured randomly in six random locations and measured three times [25]. Total color difference (ΔE) was calculated according to the following equation:

$$\Delta E = [(L - L^*)^2 + (a - a^*)^2 + (b - b^*)^2]^{½}$$

where L^*, a^*, and b^* are the color values of the white standard plate, and L, a, and b are the color values of film samples.

The film sample was cut into a size of 10 × 40 mm^2 and inserted into a quartz colorimeter with a channel width of 10 mm. The opacity was determined according to the method of Sun et al. [25], while the absorbance value was measured at 600 nm using a UV-visible spectrophotometer (UV-2600, Shimadzu, Kyoto, Japan). Then, the opacity was calculated using the following equation:

$$\%T = 100 \times 10^{-A}$$

$$\text{Opacity} = A_{600nm}/\delta$$

where A is the absorbance measured at 600_{nm} and δ is film thickness (mm).

2.6.3. Viscosity and pH

The viscosity change in nanoemulsion samples was measured using a Physical MCR 101 rheometer (Anton Paar, Ostfildern, Germany). Meanwhile, pH was measured using a CP-511 pH meter (Lasec®, Cape Town, South Africa).

2.6.4. Determination of Moisture Content and Film Water Solubility

The mass loss of 1 g of film after 24 h of oven drying at (105 ± 1) °C was used to determine the moisture content and expressed as the percentage of initial film mass loss during drying [23]. The analysis was performed three repetitive times to make each film, and the results were expressed as the mean value ± standard deviation. The water solubility of films was measured using a method described by Galus and Kadzińska [23] with at least five repetitions. Samples were dried at 105 °C for 24 h to determine their initial dry matter. The films were then immersed in distilled water in a sealed beaker at 25 °C for 24 h, with occasional stirring. After this, the films were rinsed and dried again to measure the remaining dry matter. The difference between the initial and remaining dry matter was used to calculate the percentage of dry matter dissolved in water

2.6.5. Water Vapor Permeability

The WVP of films was determined according to a method described by Elshamy et al. [26]. Briefly, aluminum cups with a 6 cm internal diameter, 8.3 cm external diameter, and 1.3 cm depth were used. The cup was filled with deionized water and sealed by the films and then placed in an oven and maintained at 25 °C and 50% RH. The cup was weighed every 1 h for 10 h using an analytical weighing balance. The water vapor transmission rate (WVTR) of the films was determined by plotting the weight gained versus time. The slope of the linear portion of this plot represented the steady-state amount of water vapor diffusing through the film per unit of time. The WVTR was expressed in grams per square meter per hour. A steady weight-over-time slope yielded a regression coefficient of 0.99 or greater. Three replicates per film were tested. The WVP of films was calculated by multiplying the WVTR by the film thickness and dividing it by the water vapor pressure difference across the films. The following equations were used:

WVP ($g \cdot mm/m^2 \cdot h \cdot kPa$) = ([WVTR × L])/ΔP, for which the water vapor transmission rate (WVTR) is the slope per film area ($g/m^2 \cdot h$), L is the film thickness (mm), and ΔP is the partial water vapor pressure difference (kPa) across the two sides of the film specimen.

2.6.6. Tensile Strength and Thickness of Films

A piece of the film (3 × 5 cm) was cut, mounted, and clamped with the texture analyzer probe (EZ-SE Texture Analyzer, Shimadzu, Tokyo, Japan). The sample was stretched at a speed of 0.1 mm/s at room temperature until it broke. This was followed by the calculation of the tensile strength and elongation at the break by using stress–strain and force–distance curves, respectively [26]. The film thickness was measured using a digital caliper (RS PRO external digital) and weighed and tared against the cups used to obtain the initial weight of the film. The same cups were weighed at hourly intervals. The decrease in film weight, initial thickness, temperature, and RH was used for the WVP calculation.

Five measurements were taken at random positions around the film sample for each replicate, and the mean values were calculated [27].

2.6.7. Scanning Electron Microscopy (SEM)

The film microstructure of the pure CH and combination films was observed under a scanning electron microscope (SEM; AURIGA, Carl Zeiss) at an accelerating voltage of 5 kV. A 5 mm×5 mm sample was fixed on the support using silver paste at an angle of 90° to the surface, which allowed for the observation of the cross-section of the film [28]. Films were observed at a magnification of 500 × (surfaces) and 1500 × (cross-sections).

2.6.8. Fourier Transform Infrared Analysis (FTIR)

The FTIR spectrum of the coating was recorded using an FT-IR spectrometer equipped with a universal attenuated total reflection (ATR) accessory in the range of 4000 to 400 cm^{-1} with a resolution of 4 cm^{-1} according to the method described by Pillai et al. [28] to determine any interaction between the (S)-EO nanoemulsion and CH matrix.

2.6.9. Thermogravimetric Analysis (TGA)

TGA was determined according to Pillai and Ray [29] using a TG-Q500 analyzer (TA Instruments, New Castle, DE, USA). Here, 10 mg of sample was heated to 900 °C at 10 °C/min under an air atmosphere (60 mL/min). The primary weight loss of the film samples as a function of temperature was recorded.

2.7. In Vivo Antifungal Activity of (S)-EO Nanoemulsion–CH Coating Formulation

Two mandarin cultivars ('Nova', 'Tango') of soft citrus fruits were surface sterilized using a 0.01% NaOCl solution for 1 min and then air dried for 20 min. Each fruit was

wounded on the surface with a sterile needle (5 mm depth × 2 mm width) on the equatorial side [9]. Approximately 6 µL of (5×10^6 spores/ µL) *P. digitatum* or *P. italicum* spore suspension was inoculated into the wound separately. After incubating at 25 °C for 8 h, the inoculated fruits were dipped in (S)-EO (2%) nanoemulsion–CH (0.8%) coating (treatments) or dipped in distilled water (control) and Imazalil for 1 min and then air dried. There were three replicate boxes, each containing 15 fruits, and each box was inoculated with a citrus pathogen. All uncoated and coated fruits were stored at 10 °C and 85 % RH for 14 days and thereafter at 18 °C for up to 5 days. The decay severity of the rotten fruit was assessed based on the developed scale: 1 = no infection; 2 = mild infection (1%–25% of the area covered by slight necrotic and fungal mycelia); 3 = moderate infection (26%–50% of the fruit area covered by necrotic and fungal mycelia); 4 = severe infection (51%–75% of the fruit is necrotic with spore masses); 5 = very severe (100% of necrotic tissue with fungal mass and the fruit appears soft and decayed), as shown in Supplementary Figure S1.

2.8. Statistical Analysis

The effectiveness of the treatments was assessed using the *Genstat* version 10th edition (VSN International, Hempstead, UK) software for analysis of variance (ANOVA). Fisher's protected test was utilized to determine significant differences between the mean values at $p < 0.05$). A *t*-test was performed in relation to physico-chemical properties to determine significant differences between the mean values at $p < 0.05$. The experiments were repeated twice using a completely randomized design for in vitro and in vivo experiments.

3. Results and Discussion

3.1. In Vitro Antifungal Effects of (S)-EO Nanoemulsion–CH Coating

The combined effects of edible coatings, (S) nanoemulsion–CH, and CH or (S)-EO nanoemulsion alone on *P. digitatum* and *P. italicum* radial mycelial growth after 7 days are illustrated in Table 1. *P. digitatum* and *P. italicum* were completely inhibited by the (S)-EO nanoemulsion at 1%. Therefore, the MIC of the (S)-EO nanoemulsion was 1% for both pathogens. However, the radial mycelial growth of *P. digitatum* was not inhibited by CH alone at concentrations ranging from 0.2% to 1% (2000–10,000 mg/L). Furthermore, 0.2% to 1% concentrations of CH alone inhibited the radial mycelial growth of *P. italicum* by less than 50%. Increasing the concentration of CH, however, resulted in a greater inhibition of the radial mycelial growth of *P. italicum*. Increased chitosan concentration was not cost-effective and would affect the application on the fruit surface. The (S)-EO nanoemulsion (0.5%) incorporated at different CH concentrations of 0.2, 0.4, 0.8, and 1% showed 100% inhibition of the radial mycelial growth of *P. digitatum*. In contrast, all combined treatments with CH and (S)-EO at all concentrations tested in this study showed 100% inhibition of the radial mycelial growth in *P. italicum*. On the other hand, the (S)-EO nanoemulsion (1%) incorporated at 0.8% or 1.0% CH showed 100% inhibition of the radial mycelial growth in *P. italicum*. The term fungistatic applies to an agent that suppresses fungal growth, whereas fungitoxicity describes agents in the position of killing [30]. In this investigation, the (S)-EO nanoemulsion at 1% or 1.5% showed a fungistatic effect on the mycelial growth of *P. italicum* and *P. digitatum*. Also, the radial mycelial growth of both citrus pathogens, *P. digitatum* and *P. italicum*, were fungistatically inhibited by the (S)-EO nanoemulsion (1%) incorporated at 0.8% or 1.0% CH, respectively (Table 1). Although both fungal colonies produced from the subculture of the inhibited colonies started to grow with time, they did not reach the same size as the control PDA plates. Therefore, the results of this study suggest that the combination of the (S)-EO nanoemulsion (1%) incorporated at 0.8% or 1.0% CH would be most effective if applied throughout the postharvest process.

Table 1. Impact of spearmint nanoemulsions, chitosan, standalone treatments, or their combinations on radial mycelial growth inhibition, minimal inhibitory concentration (MIC), and toxicity after 7 days of incubation at 25 °C in vitro.

Treatment	Concentration (%)	*Penicillium digitatum* (Green Mold)			*Penicillium italicum* (Blue Mold)		
		Mycelial Growth (mm)	Inhibition (%)	Nature of Toxicity	Mycelial Growth (mm)	Inhibition (%)	Nature of Toxicity
Spearmint nanoemulsion (S)-EO	0.5	13.2 ± 0.97 ^{e}	67.27 ± 6.02 ^{b}		23.7 ± 5.9 ^{c}	35 ± 6.9 ^{c}	
	1	0 ^{f}	100 ± 2.13 ^{a}	Fungistatic	0 ^{f}	100 ^{a}	Fungistatic
	1.5	0 ^{f}	100 ± 2.12 ^{a}	Fungistatic	0 ^{f}	100 ^{a}	Fungistatic
Chitosan (CH)	0.2	43 ± 2.16 ^{b}	0 ^{c}		35.67 ± 6.64 ^{b}	29.7 ± 2.32 ^{d}	
	0.4	44.66 ± 3.68 ^{b}	0 ^{c}		30.67 ± 1.88 ^{b}	28.57 ± 2.69 ^{d}	
	0.8	36.33 ± 2.86 ^{c}	0 ^{c}		33.33 ± 3.29 ^{b}	21 ± 6.78 ^{e}	
	1	37.67 ± 0.47 ^{c}	0 ^{c}		26.67 ± 1.69 ^{c}	35 ± 2.26 ^{c}	
Tween 80	0.5	58 ± 5.54 ^{a}	0 ^{c}		47.00 ± 3.4 ^{a}	0 ^{i}	
Imazalil	0.025	0 ^{f}	100 ± 2.1 ^{a}	Fungicidal	0 ^{f}	100 ^{a}	Fungicidal
Distilled H_2O		41.4 ± 6.01 ^{d}	0 ^{c}		41.6 ± 2.01 ^{a}	0 ^{i}	
Chitosan (CH) + spearmint essential oil (S)-EO nanoemulsion coating solution	0.2% + 0.5%	0 ^{f}	100 ± 0.81 ^{a}	Fungistatic	30.5 ± 2.5 ^{b}	26.6 ± 0.6 ^{d}	
	0.2% + 1.0%	0 ^{f}	100 ± 0.81 ^{a}	Fungistatic	15.5 ± 2.4 ^{de}	39.44 ± 2.77 ^{c}	
	0.2% + 2.0%	0 ^{a}	100 ± 0.81 ^{a}	Fungistatic	16.5 ± 3.5 ^{d}	100 ± 1.16 ^{a}	Fungistatic
	0.2% + 3.0%	0 ^{f}	100 ± 0.81 ^{a}	Fungistatic	0 ^{f}	100 ± 1.16 ^{a}	Fungistatic
	0.2% + 5.0%	0 ^{f}	100 ± 0.81 ^{a}	Fungistatic	0 ^{f}	100 ± 1.16 ^{a}	Fungistatic
	0.4% + 0.5%	0 ^{f}	100 ± 0.81 ^{a}	Fungistatic	26.00 ± 2.0 ^{c}	28.5 ± 0.87 ^{d}	
	0.4% + 1.0%	0 ^{f}	100 ± 0.81 ^{a}	Fungistatic	5.00 ± 2.0 ^{e}	33.48 ± 2.23 ^{c}	
	0.4% + 2.0%	0 ^{f}	100 ± 0.81 ^{a}	Fungistatic	0 ^{f}	100 ± 9.75 ^{a}	Fungistatic
	0.4% + 3.0%	0 ^{f}	100 ± 0.81 ^{a}	Fungistatic	0 ^{f}	100 ± 9.75 ^{a}	Fungistatic
	0.4% + 5.0%	0 ^{f}	100 ± 0.81 ^{a}	Fungistatic	0 ^{f}	100 ± 9.75 ^{a}	Fungistatic
	0.8% + 0.5%	0 ^{f}	100 ± 0.81 ^{a}	Fungistatic	15.5 ± 0.5 ^{de}	56.2 ± 3.25 ^{b}	
	0.8% + 1.0%	0 ^{f}	100 ± 0.81 ^{a}	Fungistatic	0 ^{f}	100 ± 1.82 ^{a}	Fungistatic
	0.8% + 2.0%	0 ^{f}	100 ± 0.81 ^{a}	Fungistatic	0 ^{f}	100 ± 1.82 ^{a}	Fungistatic
	0.8% + 3.0%	0 ^{f}	100 ± 0.81 ^{a}	Fungistatic	0 ^{f}	100 ± 1.82 ^{a}	Fungistatic
	0.8% + 5.0%	0 ^{f}	100 ± 0.81 ^{a}	Fungistatic	0 ^{f}	100 ± 1.82 ^{a}	Fungistatic
	1.0% + 0.5%	0 ^{f}	100 ± 0.81 ^{a}	Fungistatic	5.00 ± 1.0 ^{e}	100 ± 0.0 ^{a}	Fungistatic
	1.0% + 1.0%	0 ^{a}	100 ± 0.81 ^{a}	Fungistatic	0 ^{f}	100 ± 0.0 ^{a}	Fungistatic
	1.0% + 2.0%	0 ^{f}	100 ± 0.81 ^{a}	Fungistatic	0 ^{f}	100 ± 0.0 ^{a}	Fungistatic
	1.0% + 3.0%	0 ^{f}	100 ± 0.81 ^{a}	Fungistatic	0 ^{f}	100 ± 0.0 ^{a}	Fungistatic
	1.0% + 5.0%	0 ^{f}	100 ± 0.81 ^{a}	Fungistatic	0 ^{f}	100 ± 0.0 ^{a}	Fungistatic

The means in columns with different letters are significantly different by Fisher's protected test ($p < 0.05$) applied after ANOVA. Colony diameter reduction concerning control treatments (non-amended plates). Mean values with similar alphabets in a column are not significantly different at $p < 0.05$.

The effectiveness of the (S)-EO nanoemulsion on the spore germination of *P. digitatum* and *P. italicum* is given in Figure 1. A 100% spore germination inhibition was observed in *P. digitatum* when the 2% (S)-EO nanoemulsion was applied. In contrast, the 1% (S)-EO nanoemulsion showed 100% *P. italicum* spores. The (S) nanoemulsion showed EC_{50} values of 250 mg/L and 300 mg/L for *P. digitatum*, while the combinations of the CH and (S) nanoemulsion showed IC_{50} values of 250 mg/L for *P. digitatum* and a lower IC_{50} value of 110 mg/L for *P. italicum* (Table 2). A study by Zulu et al. [31] found that cinnamon EO had an IC_{50} value of 0.42 µL/mL for *P. digitatum*, which was higher than the IC_{50}

reported in this study. The decrease in the IC_{50} value of the (S)-EO nanoemulsion when incorporated into CH may suggest effective penetration and interaction of the active components with the target microbial cells [24], leading to higher potency of the substance at a lower concentration. Higher concentrations of EOs should have stronger inhibitory effects, but the effectiveness may differ depending on the type of EO. Some EOs are highly effective at low concentrations, while others require high concentrations, which may affect other properties of the coatings [31]. The antifungal properties of spearmint oils reduced sporulation in *P. digitatum* [32]. As spores are the primary means of transmitting infection throughout the postharvest chain, the antifungal effect of the oils as well as their ability to reduce spore germination may be as critical to the control of blue and green mold decay in soft citrus fruits.

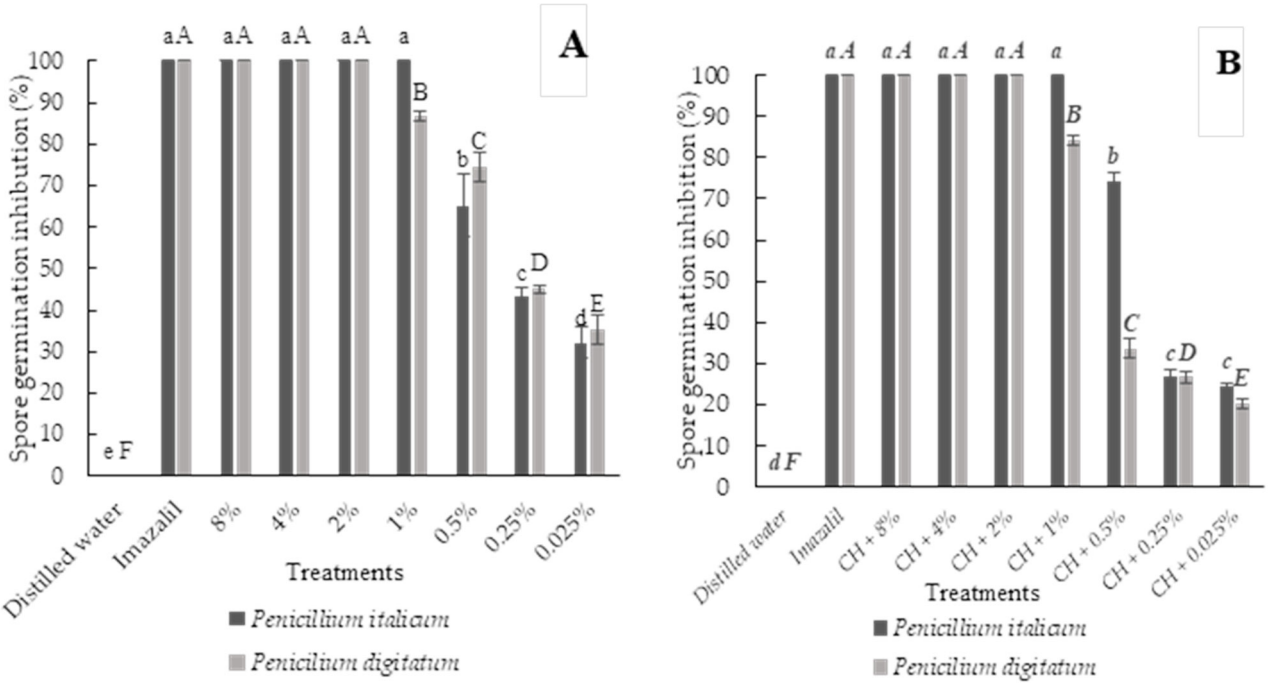

Figure 1. Spore germination inhibition percentage of (**A**) spearmint nanoemulsion essential oil and (**B**) a combination of chitosan (CH) at 0.8% and various spearmint EO nanoemulsion concentrations, including Imazalil (positive control) at 250 mg/L and distilled water (negative control) incorporated into PDA plates on the growth of *Pencillium italicum* and *Penicillium digitatum* after 72 h incubation at 25 °C. The bars depict the means, and the error bars illustrate the standard deviations associated with the means. Small and capital letters indicate significant differences among the treatments for *Penicillium italicum* and *Penicillium digitatum*, respectively, according to Fisher's protected test ($p < 0.05$) applied after ANOVA.

Table 2. Half maximal effective concentrations (EC_{50}) for spearmint (S) nanoemulsion and chitosan (CH) + (S) nanoemulsion evaluated against *Penicillium digitatum* and *Penicillium italicum*.

EO-Emulsion	Pathogen	EC_{50} (mg/L)	Toxicity Regression Equation	R^2
(S) nanoemulsion	*Penicillium digitatum*	240	y = 0.548× + 36.045	0.9061
	Penicillium italicum	300	y = 0.0705× + 28.696	0.9747
CH + (S) nanoemulsion	*Penicillium digitatum*	250	y = 0.0633× + 33.519	0.9321
	Penicillium italicum	110	y = 0.0587× + 43.239	0.9556

The results indicate that spore germination decreases as the concentrations increase (Figure 1), which is consistent with the inhibition of radial mycelial growth results. The nanoemulsion used in this study has a smaller particle size, which allows easier penetration into cell membranes. Its pronounced antifungal activity can be attributed to its

abundance of oxygenated monoterpenes, particularly carvone, which has shown antifungal properties [14]. Essential oil components may affect enzyme reactions involved in fungus cell wall synthesis, affecting fungal growth and morphogenesis [31]. *P. digitatum* hyphal morphology was altered following treatment with clove oil as reported by Yahyazadeh et al. [33]. Tao et al. [34] also observed cytoplasmic loss and distortion in *P. italicum* and *P. digitatum* upon the application of *Citrus reticulata* Blanco essential oil. Even though essential oils' antifungal activity is unclear, it has been hypothesized that their lipophilicity in nano formulations facilitates their separation from water, allowing them to easily integrate with pathogen membranes [34]. According to our SEM observations, the spores of both pathogens showed detrimental effects on the spores (unpublished data). (S)-EO nanoemulsion and CH and (S)-EO nanoemulsion have fungitoxic effects. The structure and composition of fatty acids in sensitive fungi species change, and vacuoles are formed in their cells. Meanwhile, cell membrane synthesis and repair are suppressed, impairing cell division, growth, and spore formation [35].

3.2. Particle Size, Polydispersity Index (PDI), and Zeta Potential of Spearmint EO-CH Coating

Table 3 shows the particle size, polydispersity index (PDI), and zeta-potential (Z) of pure CH, the (S)-EO nanoemulsion, and the (S)-EO nanoemulsion–CH coating solution. These parameters indirectly determine various properties and activities of emulsions, such as stability, encapsulation efficiency, bioactive compound release profiles, and rheological behavior [23]. The particle size of CH was 159.2 nm, which increased to 252.3 nm with (S)-EO nanoemulsion incorporation. (S)-EO nanoemulsion (1.5%) alone had a particle size of 88.93 nm. Microemulsions typically have particle sizes of 10 to 50 nm, while nanoemulsions have particle sizes of 50 to 500 nm [36]. The results indicated that the (S)-EO nanoemulsion and the corresponding coating formulation conformed to the nanoemulsion range, and these results are consistent with those of de la Cruz et al. [37], who investigated (S)-EO nanoemulsions' formation with different emulsifying agents. The increase in particle size of CH after the incorporation of (S)-EO, interestingly, is in agreement with Tariq et al. [38], who noted that a slight reduction in the oil–polysaccharide interfacial energy can significantly influence nanoemulsion particle size, suggesting that the incorporation of the (S)-EO nanoemulsion in the system did not prevent coalescence, leading to larger particle sizes.

Table 3. Particle size, PDI, and zeta potential of 2% spearmint nanoemulsion and nanoemulsion, 0.8% chitosan, and their combination. Values are shown as mean ± standard deviation (SD). The means in columns with different letters are significantly different by Fisher's protected test at $p < 0.05$. *ND—no data.

Treatment	Particle Size (nm)	PDI	Z-Potential (mV)	Viscosity (Pa.s)	pH
0.8% CH	159.2 ± 11.79 ^{b}	0.83 ± 0.06 ^{a}	42.16 ± 1.47 ^{a}	15.16 ± 0.27 ^{a}	4.08 ± 0.01 ^{a}
CH + (S)-EO nanoemulsion	252.3 ± 97.57 ^{a}	0.61 ± 0.06 ^{c}	21.6 ± 4.62 ^{b}	9.35 ± 0.19 ^{b}	4.16 ± 0.01 ^{a}
1.5% (S)-EO nanoemulsion	88.93 ± 15.47 ^{c}	0.74 ± 0.08 ^{b}	14.56 ± 1.04 ^{c}	*ND	4.1 ± 0.01 ^{a}

PDI values which indicate the uniformity of particle size distribution were 0.83, 0.61, and 0.74, respectively, for CH, the (S)-EO nanoemulsion–CH formulation, and the (S)-EO nanoemulsion alone (1.5%) (Table 3). The results indicated more stable and regular size distributions of the prepared coating formulation when compared to CH and (S) EO(S)-EO nanoemulsions individually. However, the PDI values were found to be higher than those reported by Tariq et al. [38] who reported values below 0.4 for the (S) EO nanoemulsion encapsulated in CH using citric acid cross-linking.

The zeta potential value (Table 3), which measures the stability of colloidal systems, decreased from +14.56 mV for the (S)-EO nanoemulsion to +21.6 mV after the incorporation

into CH, indicating an electrostatic stabilization effect. On the other hand, CH on its own had zeta potential of +42.16 mV, which reduced after the incorporation of the (S)-EO nanoemulsion. This observation is in line with that of Yousef et al. [39] who suggested that the adsorption of EO on the particle surfaces masked the free NH^{3+} groups of CH and decreased surface charge. In nanoemulsions, zeta potential values above ±30 mV are optimal for emulsion stabilization [40]. In this case, the EO stabilized through a Pickering mechanism on the surface of CH particles, which could have decreased zeta potential [38,39]. This increase in the particle size of CH is consistent with this observation (Table 3). Further analyses of the performance of the coating formulation indicated that the reduction in the zeta potential did not affect its microbial protection efficacy.

3.3. Viscosity and pH of (S)-EO Nanoemulsion–CH Coating

Table 3 shows the viscosity and pH values of the CH coating formulation with the (S)-EO nanoemulsion and the (S)-EO nanoemulsion alone. Incorporation of the (S)-EO nanoemulsion significantly decreased the viscosity of CH from 15.16 Pa·s to 9.35 Pa·s. As a result, the film-forming solution used in the coating became less viscous, which could be advantageous for the spray coating technique. The adsorption of the (S)-EO nanoemulsion on the CH surface might have reduced the resistance to the flow and hence reduced viscosity. The observations agree with the reduction in the viscosity of the CH coating film formulations after the incorporation of 1% basil and thyme EO observed by Bonilla et al. [41]. For (S)-EO nanoemulsions, viscosity did not show a value consistently due to their Newtonian behavior, where viscosity remains unchanged with increasing shear rates [41].

Additionally, Elshamy et al. [26] reported similar results when CH film formulations were incorporated with increasing concentrations of thyme nanoemulsion, suggesting interactions between CH and nanoemulsion components play a crucial role in determining the rheological properties of film-forming solutions. The pH of a coating influences its antimicrobial activity, as it influences how it interacts with microbial cells [41]. In this study, the pH of the treatments stayed within an acidic range, specifically between 4.16 and 4.08 (Table 3). The (S)-EO nanoemulsion did not alter the pH of the CH-based coating. According to Hong et al. [35], acidic conditions facilitate electrostatic interactions between positively charged amino groups (NH^{3+}) in CH and negatively charged surfaces in fungal cells. In addition to increasing permeability and osmotic imbalance, these interactions can inhibit fungal growth according to Hong et al. [41].

In low-pH conditions, the protonation of amino groups in CH enhances its antimicrobial efficacy, and the coatings enhance their antimicrobial efficacy, as electrostatic interactions with fungal cell surfaces are strengthened, thereby disrupting cell membrane integrity (Hong et al.) [42]. By inhibiting the growth of spoilage fungi, an acidic environment can extend the shelf life of food products during preservation. The (S)-EO nanoemulsion did not alter the pH, suggesting that the active compounds in (S)-EO can enhance the antimicrobial properties of the CH coating without compromising its structure or functionality (Table 3). This finding is consistent with a growing body of research emphasizing pH's role in modulating the antimicrobial activity of biopolymer-based coatings, particularly those using EOs as nanoemulsions. Using a plant-based nanoemulsion to enhance the natural antimicrobial properties of CH provides a promising strategy for developing effective natural antifungal coatings.

3.4. Color and Opacity of (S)-EO Nanoemulsion–CH Coating

The optical properties of the CH film and the (S)-EO nanoemulsion and CH coating film are given in Table 4. Color is a key factor in consumer acceptance of edible coatings.

Color measurements showed a decrease in *L** values from 87.03 for pure CH to 75.75 for CH incorporated with the (S)-EO nanoemulsion. This decline in lightness was even more pronounced for the (S)-EO nanoemulsion alone, which had an *L** value of 54.06. This was likely caused by the essential oil droplets dispersed within the polymeric CH matrix [23].

Table 4. Optical properties of spearmint nanoemulsion and chitosan coating.

Coating	L*	a*	b*	ΔE	Opacity (A/•mm^1)
Chitosan (0.8%)	87.03 ± 5.21 ^{a}	0.56 ± 0.32 ^{a}	3.58 ± 1.13 ^{b}	*ND	0.504 ± 0.04 ^{a}
Chitosan (0.8%) + 2% Spearmint nanoemuslion	75.75 ± 0.08 ^{b}	0.29 ± 0.05 ^{c}	3.91 ± 0.51 ^{a}	14.14 ± 9.16	0.562 ± 0.05 ^{a}
2% Spearmint nanoemulsion	54.06 ± 6.11 ^{c}	0.51 ± 0.14 ^{b}	1.75 ± 0.32 ^{c}	*ND	*ND

Data expressed as mean ± standard deviation of three replicates. The means in columns with different letters are significantly different by Fisher's protected test at $p < 0.05$. L*—lightness, a*—redness, b*—yellowness. *ND—no data.

Moreover, the *b** values increased slightly from 3.58 to 3.91 with the incorporation of the (S)-EO nanoemulsion, indicating a shift toward a more yellow hue. Similarly, de Oliveira Filho et al. [43] found similar changes in CH films when *Citrus limonia* EO was added, indicating a common interaction between EOs and CH. CH incorporated with the EO nanoemulsion showed a total color difference of 14.14, suggesting that despite the noticeable color changes, the essential oil did not drastically alter the optical properties.

As shown in Table 4, the (S)-EO nanoemulsion reduced the transparency of pure CH films (from 55.37 to 50.72%). A food's opaqueness affects how light interacts with it, thus influencing its appearance, and a similar report on the incorporation of citrus EO reducing light transmission and increasing opacity in gelatine films can be found in the literature [23]. A decrease in transparency could be advantageous as it could be associated with improved barrier properties against UV light [44]. Edible coatings' ability to block UV light is not only important for appearance but also for oxidative stability. UV barrier properties delay the oxidative degradation of lipids, preserving nutritional quality and extending shelf life [23]. Incorporating an (S)-EO nanoemulsion into CH films creates protective barriers that reduce nutrient loss and deterioration caused by UV light, enhancing edible coating functionality [23].

3.5. Thickness, Moisture Content, Water Solubility, Tensile Strength, and Water Vapor Permeability (WVP) of Spearmint (S)-EO Nanoemulsion–CH Coating

Coating thickness and tensile strength are determined for a variety of reasons. Coating mechanical performance is determined by its ability to resist stress without cracking. Higher tensile strength indicates the durability and reliability of a coating [44]. Among barrier properties, thickness plays an important role in influencing moisture and gas protection. Inconsistencies in the coating process may result in variations in thickness, resulting in weak points or compromised barrier properties [45]. A tensile test can be useful for determining the integrity and consistency of a coating, offering insight into the quality of the coating material as well as the efficiency of the application method [45,46]. Table 5 illustrates the (S)-EO nanoemulsion's impact on the physical properties of the CH coating. The thickness of the CH film increased from 0.021 mm to 0.024 mm with the addition of the (S)-EO nanoemulsion. This increase in thickness can be attributed to the larger number of molecules in the coating matrix and the increased particle size observed with the nanoemulsion incorporation, and Zhang et al. [47] observed significant increases in CH film thickness after adding cinnamon essential oil. Likewise, de Oliveira Filho et al. [43] noted that increasing concentrations of citrus EO led to a substantial increase in CH film thickness. These results suggest that covalent bonds form between the functional groups of CH and

the EO chains when the EO is integrated into CH films. Such bonds could also decrease the coating's porosity, potentially improving its ability to protect food surfaces [43].

Table 5. Physico-chemical properties of chitosan and chitosan–spearmint oil nanoemulsion films.

Treatment	Thickness (mm)	Moisture Content (%)	Water Solubility (%)	WVP (g·mm/m^2·h·kPa)	Tensile Strength (MPa)
(0.8%) CH	0.021 ± 0.01 ^{b}	69.71 ± 6.31 ^{a}	44.26 ± 0.75 ^{b}	0.01 ± 0.00 ^{a}	19.49 ± 5.10 ^{a}
CH + (S)-EO nanoemulsion	0.024 ± 0.01 ^{a}	65.84 ± 1.84 ^{b}	58.11 ± 6.81 ^{a}	0.02 ± 0.00 ^{a}	14.39 ± 1.49 ^{b}

Values are shown as mean ± standard deviation (SD). Different letters in the same column indicate significant differences during *t*-test at $p < 0.05$. WVP: water vapor permeability. g·mm/[m^2-h]: grams. millimeters/meter square-hour. MPa: megapascal.

As shown in Table 5, the (S)-EO nanoemulsion–CH coating had moisture content of 65.71%, compared with 69.71% for pure CH. This reduction is likely due to the hydrophobic nature of the essential oil, which repels water and therefore decreases the coating's water retention capacity [43]. High moisture levels can compromise both the film and packaged product's durability in edible coatings. Higher moisture content in the film increases susceptibility to microbiological damage, while lower moisture content can extend protection periods.

Water solubility increased from 44.26% in the CH film to 58.11% in the (S)-EO nanoemulsion–CH coating (Table 5). Adding a nanoemulsion may have disrupted the polymer chains, increased hydroxyl groups, and thus increased the water solubility. In contrast, Lee et al. [48] reported that guar gum/mung bean starch films containing 2% sunflower oil displayed 34.80% water solubility. It is also important to consider the role of the surfactant, particularly Tween 80, with its high hydrophilic–lipophilic balance (HLB). Likely, Tween 80 enhanced the solubility of the EO nanoemulsion, and this illustrates the importance of intermolecular interactions between EO components and polymer hydroxyl groups, which influence their interaction with water molecules [49].

Table 5 shows the water vapor permeability (WVP) of CH and the (S)-EO nanoemulsion–CH coatings. Incorporating the (S)-EO nanoemulsion into CH film had no significant impact on WVP, with both coatings showing low WVP values of 0.01 and 0.02 g·mm/m^2·h·kPa. According to Nazari et al. [50], EO can reduce WVP by increasing the hydrophobicity of film structures and lowering the WVP values due to densely packed lipid molecules, creating an indirect path for water molecules and thus inhibiting the transmission of water molecules. The findings suggest that EO nanoemulsions can effectively prevent water vapor transfer in coatings.

The tensile strength of packaging films is one of the most important properties of these films [27]. The inclusion of an (S)-EO nanoemulsion reduced CH's tensile strength from 19.49 MPa to 14.49 MPa (Table 3). The reduction may have been caused by a weakened polymer matrix, which increases free volume and molecular mobility due to disrupted interpolymer linkages [27]. There is well-documented evidence that such disruptions can reduce cohesion and tensile strength, although they may improve flexibility [19], which indicates possible interactions of the EO nanoemulsion with CH, contributing to the emulsification of the system. Previously, CH films incorporated with EO had reduced tensile strength [51].

3.6. Surface Morphology of (S)-EO Nanoemulsion–CH Coating

Pure CH coatings and films incorporated with (S)-EO nanoemulsion are shown in (Figure 2A–D). Pure CH films were flat, consistent, and tightly structured, indicating excellent film-forming ability. As a result of its barrier properties and mechanical strength, CH is used in a wide range of applications, including drug delivery and food packaging [42].

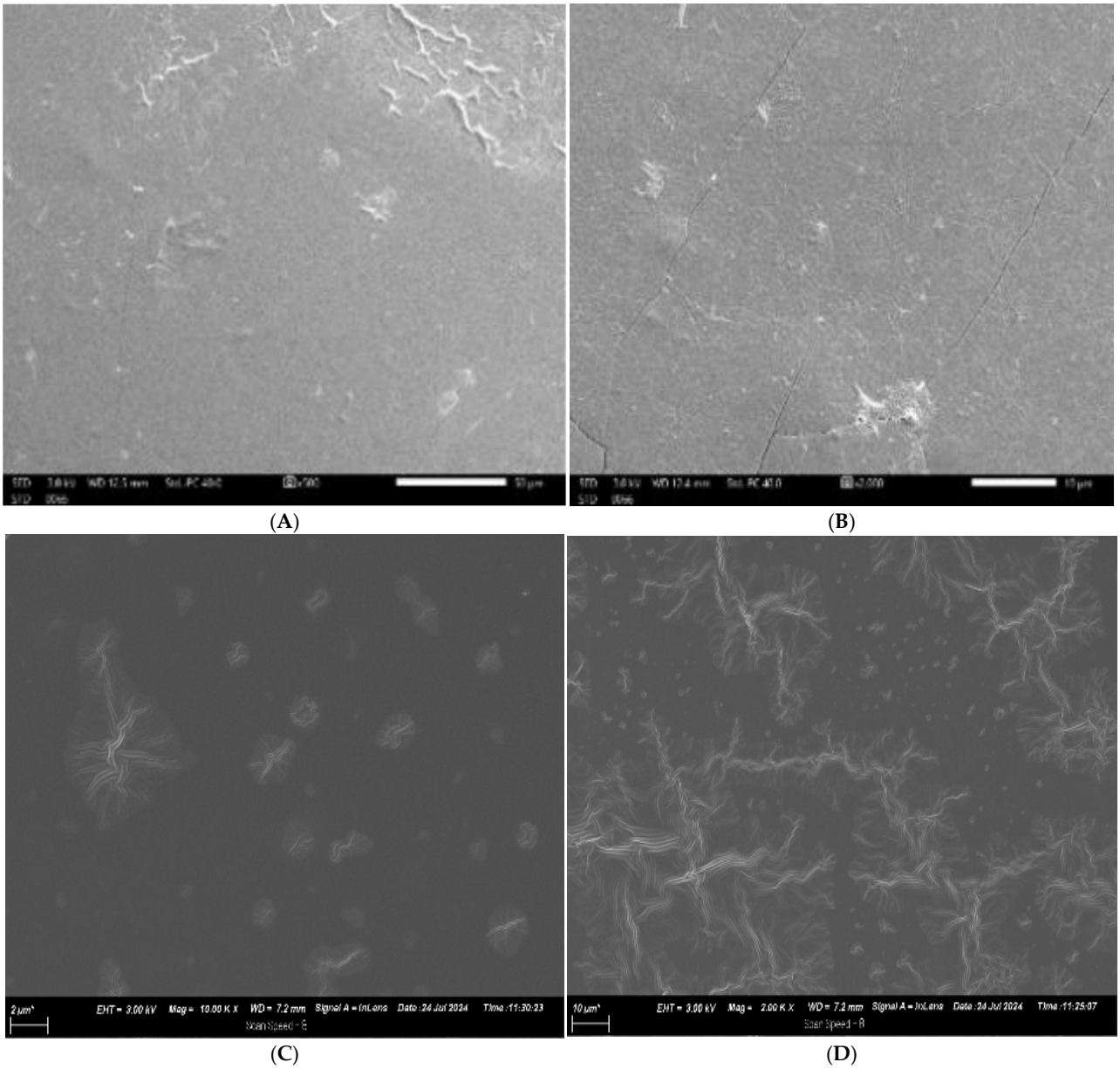

Figure 2. Morphology of chitosan and chitosan with spearmint nanoemulsion films by SEM. Chitosan (**A**) at 500×, (**B**) at 2000×; chitosan with 2% spearmint nanoemulsion (**C**) at 500×, (**D**) at 2000×.

The morphology of CH films incorporated with (S)-EO nanoemulsions (Figure 2C,D) revealed a notably different surface structure with a coarse texture and pronounced bulges. CH films incorporated with only a plasticizer exhibited similar morphological features, such as bulges, pores, and slight cracks [51]. Nanoemulsions disrupt the uniformity of the CH matrix, resulting in these surface irregularities. It appears that the type of EO plays a significant role in determining the final morphology of films incorporated with ginger EO and plasticizer [51].

In contrast, Elshamy et al. [26] found smoother surfaces in CH films incorporating thyme nanoemulsions than in pure CH films. This discrepancy may be due to specific interactions between the EO components and the CH matrix. In a nanoemulsion containing EOs, the type of oil used impacts the degree of plasticization of glycerol and the film-forming ability of CH, resulting in variations in the surface properties [50,51]. The presence of different EOs could alter the compatibility between the nanoemulsion and CH matrix, resulting in smoother or coarser surface surfaces based on chemical interactions [51].

These findings suggest that EOs can significantly alter the surface morphology of CH films, which can have implications on their mechanical properties, barrier performance, and applications in food preservation.

3.7. Fourier Transform Infrared Spectroscopy (FTIR) of (S)-EO Nanoemulsion–CH Coating

The intermolecular interactions between the (S)-EO nanoemulsion and CH were assessed by analyzing changes in the intensity and position of the peaks in the FTIR spectra (Figure 3). The spectra of both samples displayed characteristic peaks at 3292/cm and 3302/cm, corresponding to CH and linked to O-H stretching vibrations, respectively. Broad peaks observed at 2918/cm and 2928/cm were also characteristic of CH, associated with C-H stretching vibrations [27].

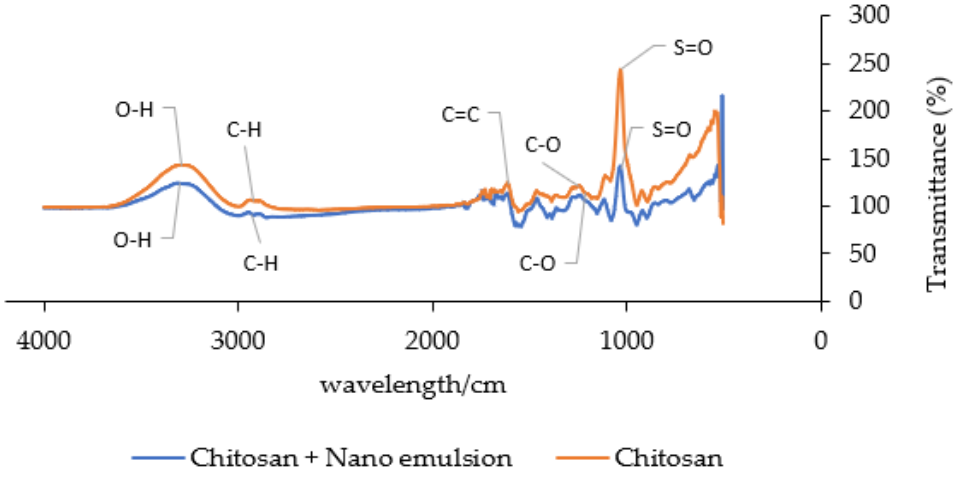

Figure 3. Fourier transform infrared spectroscopy (FTIR) spectra of chitosan and chitosan with nanoemulsion.

The incorporation of an (S)-EO nanoemulsion into the CH matrix resulted in a decrease in the intensity of the O-H stretching, C-H stretching, and C-O stretching vibrations at 3292/cm, 2918/cm, and 1212/cm, respectively. The reductions are indicative of the encapsulation of the EO nanoemulsion in the CH matrix and the interaction with the polymer, which will decrease the band intensities. Furthermore, no peak shift to lower wave numbers was observed, which is a hallmark of hydrogen bond formation between CH and the (S)-EO nanoemulsion [52]. These results suggest efficient loading of the (S)-EO nanoemulsion onto the CH polymer surface but do not indicate any covalent interaction between the (S)-EO nanoemulsion components and CH [52].

The absence of new peaks or significant changes in the FTIR spectra could also reaffirm that the interaction between CH and the (S)-EO nanoemulsion is non-covalent, primarily relying on physical entrapment and hydrogen bonding rather than chemical crosslinking [52]. These findings highlight the effectiveness of CH as a carrier for the (S)-EO nanoemulsion, preserving the integrity of both components while facilitating their combination into a stable coating material.

3.8. Thermal Stability of (S)-EO Nanoemulsion–CH Coating

Thermogravimetric analysis (TGA) was employed to evaluate the thermal stability of CH and CH coatings incorporated with (S)-EO nanoemulsions, as depicted in Figure 4A,B. The TGA profiles revealed a three-stage thermal decomposition process for both CH and the (S) EO-CH coating.

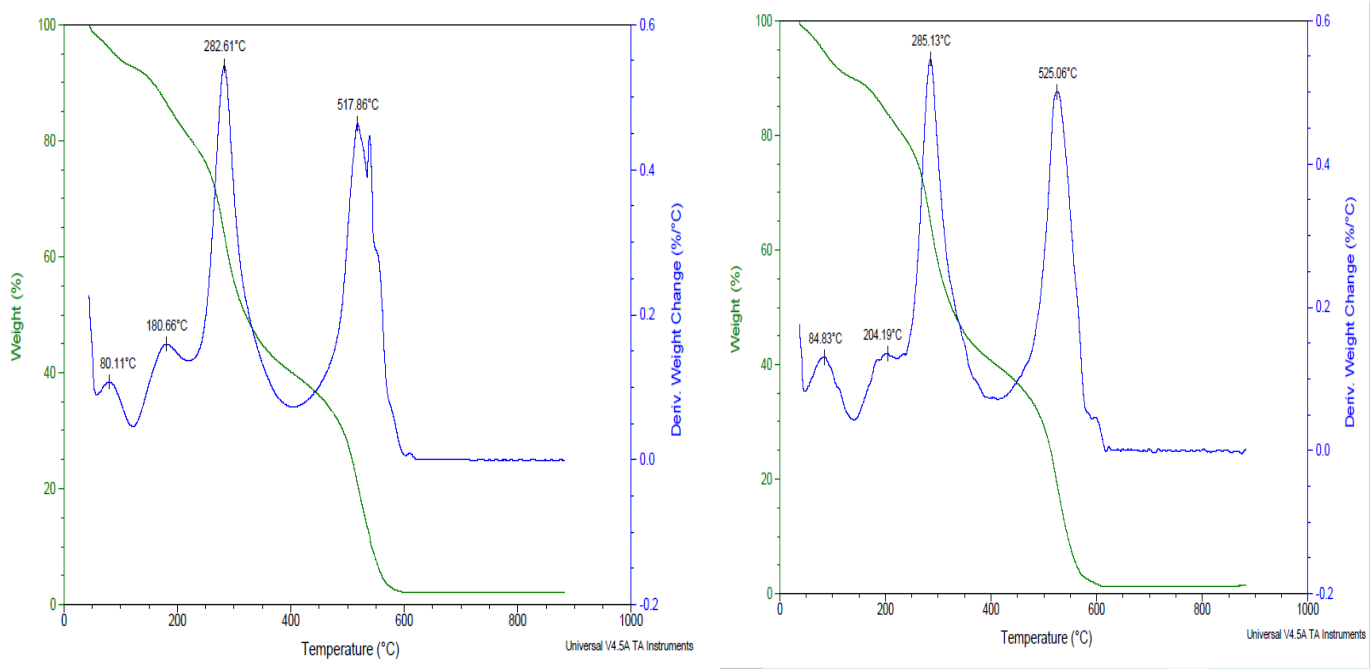

(**A**) (**B**)

Figure 4. Thermogravimetric analysis (TGA) of (**A**) chitosan and (**B**) spearmint CH + EO coating (chitosan + nanoemulsion).

In the first stage, weight loss occurred within the temperature range of 80.11–180.66 °C for pure CH, while the range shifted to 84.83–204.19 °C upon the incorporation of the (S)-EO nanoemulsion. This initial weight loss corresponds to the drying stage, where the evaporation of water molecules occurs, a phenomenon consistent with the findings of Mao et al. [53]. The second stage of thermal decomposition was observed at 180.66–282.61 °C for CH and 204.19–285.13 °C for the (S)-EO nanoemulsion–CH coating. This stage is characterized by the devolatilization of the CH substrate and the evaporation of glycerol, a plasticizer often used in the formation of biopolymer films, with a boiling point of approximately 198 °C, as reported by Liu et al. [54]. The shift to higher temperatures in the (S)-EO nanoemulsion–CH coating suggests enhanced thermal resistance, possibly due to interactions between the CH matrix and the (S)-EO nanoemulsion components.

3.9. In Vivo Antifungal Effects of (S)-EO Nanoemulsion–CH Coating

The results of green and blue mold decay of soft citrus cultivars 'Tango' and 'Nova' are illustrated in Figures 5 and 6. The decay incidence and severity were significantly different for both soft citrus cultivars inoculated with *P. digitatum* (green mold) and *P. italicum* (blue mold) between the coating group and the control (untreated fruit). The (S)-EO nanoemulsion–CH coating reduced green mold decay on both soft citrus cultivars by 100% compared to the control, similar to the Imazalil fungicide. Du Plooy et al. [55] demonstrated that fruit coatings combined with *M. spicata* at 0.25% produced as well as the fungicide controls in an in vivo trial.

However, *P. italicum* (blue mold) decay was reduced to 33% and 18% in 'Nova' and 'Tango' soft citrus compared to the control (Figures 7–9). The decay severity in both soft citrus cultivars was scale 1, indicating 1%–25% of the area is covered by necrotic and fungal mycelia (Figure S1). In contrast, Imazalil showed 100% control of green and blue mold in soft citrus cultivars (Figure 6(A2,B2)). The antifungal activity of spearmint essential oil has been reported to be effective against *Penicillium* sp. However, in this study, the (S)-EO

nanoemulsion and the (S)-EO nanoemulsion–CH formulation showed different antifungal activities against blue and green mold (Figures 7–9).

Figure 5. Impact of spearmint EO nanoemulsion-loaded chitosan coating on the (**A**) blue mold (*P. italicum*) and (**B**) green mold (*P. digitatum*) incidence after inoculation in *Citrus reticulata* 'Tango' after storage at 10 °C and 85 % RH for 14 days and, after that, at 18 °C for up to 5 days. 1—control; 2—Imazalil; 3—chitosan (0.8%); 4—CH + 1% (chitosan (0.8%) + 1% spearmint EO nanoemulsion); 5—CH + 1.5% (CH (0.8%) + 1.5% spearmint EO nanoemulsion); 6—CH + 2% (CH (0.8%) + 2% spearmint EO nanoemulsion).

Figure 6. Impact of spearmint EO nanoemulsion-loaded chitosan coating on the (**A**) blue mold (*P. italicum*) and (**B**) green mold (*P. digitatum*) incidence after inoculation in *Citrus reticulata* 'Nova' after storage at 10 °C and 85 % RH for 14 days and, after that, at 18 °C for up to 5 days. 1—control; 2—Imazalil; 3—chitosan (0.8%); 4—CH + 1% (chitosan (0.8%) + 1% spearmint EO nanoemulsion); 5—CH + 1.5% (CH (0.8%) + 1.5% spearmint EO nanoemulsion); 6—CH + 2% (CH (0.8%) + 2% spearmint EO nanoemulsion).

This study also demonstrated that the cultivar type and different Penicillium species influenced the level of infection when treated with the (S)-EO nanoemulsion–CH formulation. It seems that the physical and physiological characteristics of the rind have a greater impact on host susceptibility than genetic characteristics [3]. Consequently, its application on the infected fruit surface (curative treatments) could also affect microorganism growth and metabolism. A significant number of factors determine the effectiveness of CH on decay control. These factors include molecular weight, the degree of polymerization and deacetylation, and citrus cultivar. Furthermore, the combined application of (S)-EO (2%)

nanoemulsion–CH (0.8%) must, however, be evaluated in a commercial packing line to determine its effectiveness as a postharvest biobased solution.

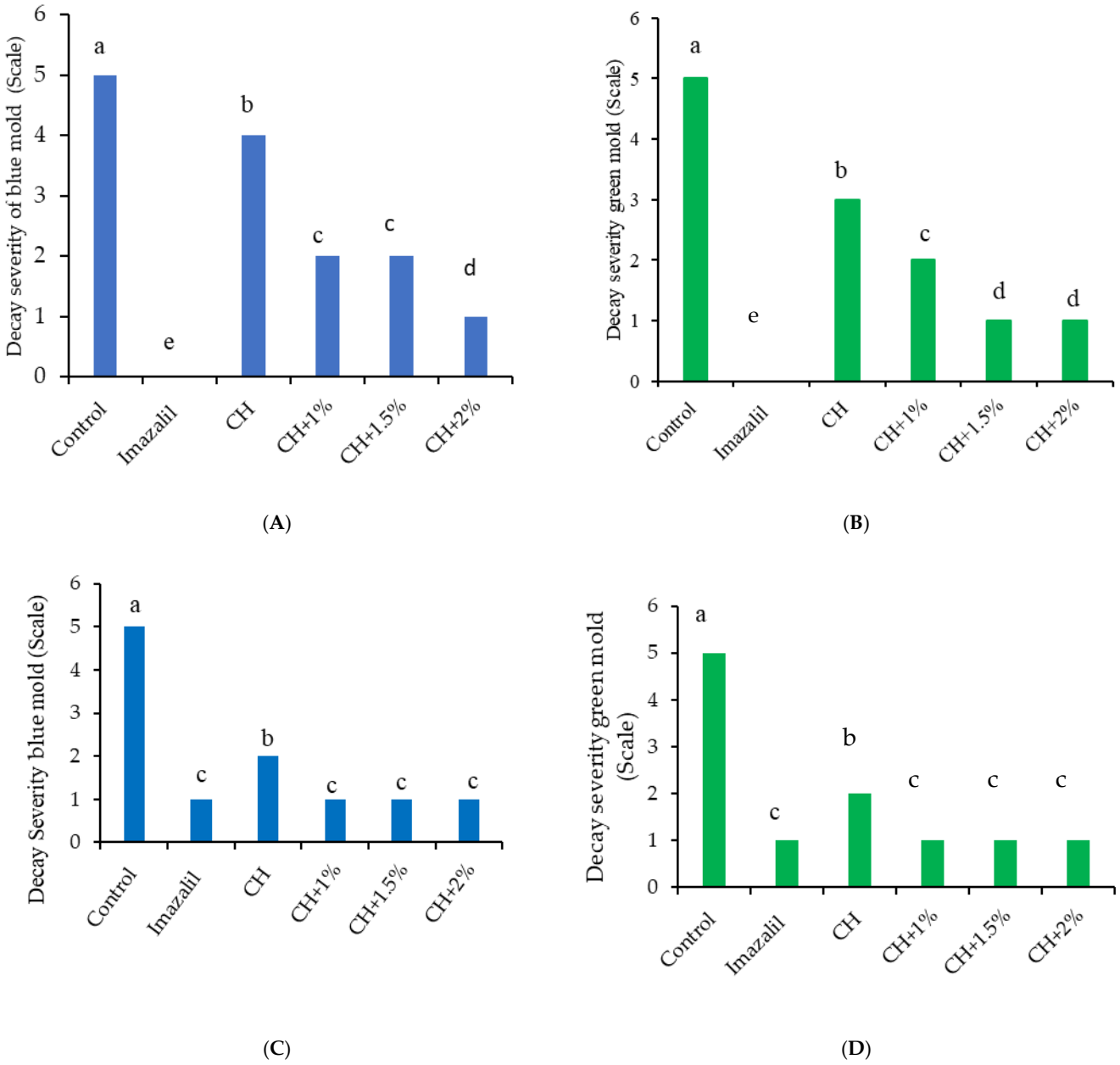

Figure 7. Impact of spearmint EO nanoemulsion-loaded chitosan coating on the (**A**) blue mold (*P. italicum*) and (**B**) green mold (*P. digitatum*) severity after inoculation in *Citrus reticulata* 'Tango' (**C**) blue mold (*P. italicum*) and (**D**) green mold (*P. digitatum*) severity after inoculation in *Citrus reticulata* 'Nova' after storage at 10 °C and 85% RH for 14 days and, after that, at 25 °C for up to 5 days. CH—chitosan (0.8%), CH + 1%—chitosan (0.8%) + 1% spearmint EO nanoemulsion, and CH + 2%—chitosan (0.8%) + 2% spearmint EO nanoemulsion. The means in columns with different letters are significantly different by Fisher's protected test at $p < 0.05$.

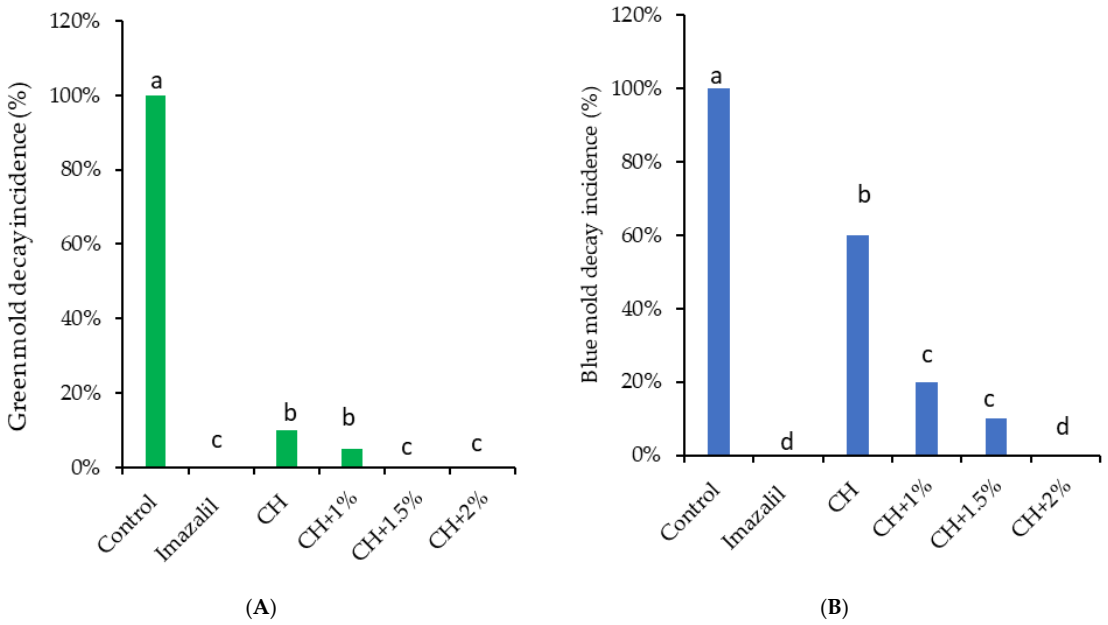

Figure 8. Impact of spearmint EO nanoemulsion-loaded chitosan coating on the (**A**) green mold (*P. digitatum)* and (**B**) blue mold (*P. italicum*) incidence after inoculation in *Citrus reticulata* 'Tango' after storage at 10 °C and 85% RH for 14 days and thereafter at 25 °C for up to 5 days. CH—chitosan (0.8%), CH + 1%—chitosan (0.8%) + 1% spearmint EO nanoemulsion, and CH + 2%—chitosan (0.8%) + 2% spearmint EO nanoemulsion. The means in columns with different letters are significantly different by Fisher's protected test at $p < 0.05$.

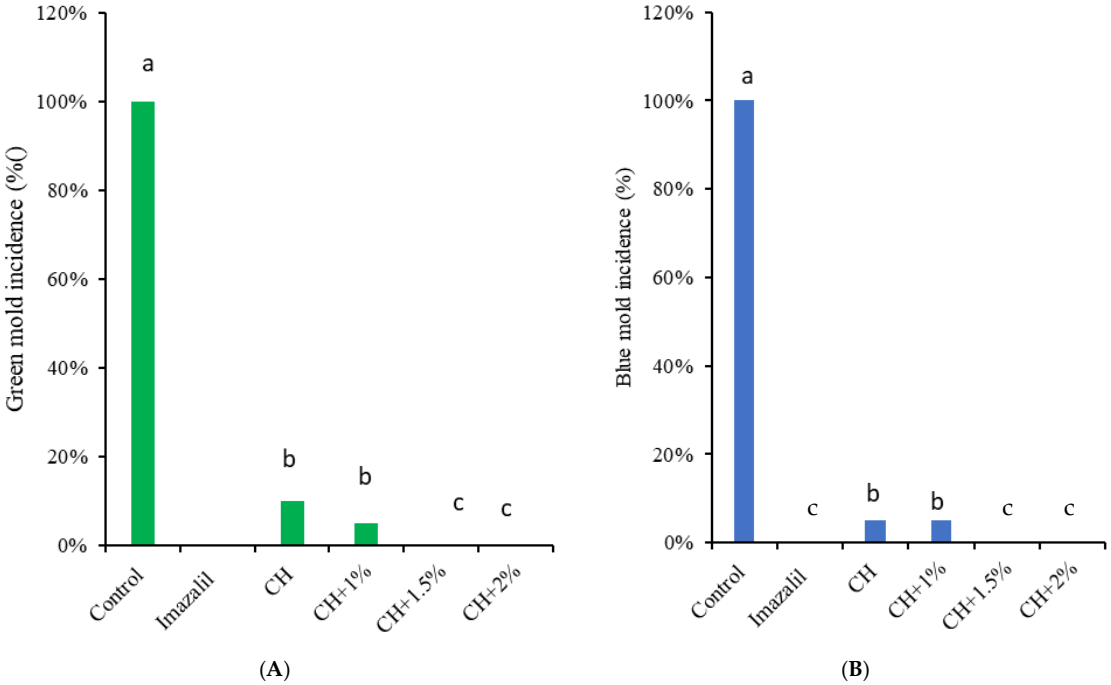

Figure 9. Impact of spearmint EO nanoemulsion-loaded chitosan coating on the (**A**) green mold (*P. digitatum*) and (**B**) blue mold (*P. italicum*) incidence after inoculation in *Citrus reticulata* 'Nova' after storage at 10 °C and 85% RH for 14 days and thereafter at 25 °C for up to 5 days. CH—chitosan (0.8%), CH + 1%—chitosan (0.8%) + 1% spearmint EO nanoemulsion, and CH + 2%—chitosan (0.8%) + 2% spearmint EO nanoemulsion. The means in columns with different letters are significantly different by Fisher's protected test at $p < 0.05$.

4. Conclusions

In this study, CH (0.8%) loaded with an (S)-EO (2%) nanoemulsion demonstrated an enhanced matrix effect on antifungal activity, inhibited the *P. digitatum* and *P. italicum* decay, and protected the soft citrus fruits compared to the control. Thus, (S)-EO nanoemulsion–CH coatings may be an effective alternative to Imazalil, reducing the environmental impact and providing an eco-friendly way to preserve the quality of soft citrus fruits after harvest.

Supplementary Materials: The following supporting information can be downloaded at https://www.mdpi.com/article/10.3390/coatings15010105/s1: Figure S1: Disease severity scale.

Author Contributions: Methodology S.K.P.; software S.K.P.; validation S.K.P.; formal analysis L.T.C.M., investigation, S.K.P., L.T.C.M. and D.S., resource S.K.P. and D.S.; data curation S.K.P. and D.S.; writing—original draft preparation L.T.C.M.; writing—review and editing S.K.P. and D.S.; visualization S.K.P. and D.S.; supervision D.S. and S.K.P.; project administration D.S., funding acquisition D.S.; Conceptualization D.S., L.T.C.M. and S.K.P. All authors have read and agreed to the published version of the manuscript.

Funding: This research was funded by the Department of Science and Innovation, the Government of South Africa, and the National Research Foundation grant number 98352.

Institutional Review Board Statement: Not applicable.

Informed Consent Statement: Not applicable.

Data Availability Statement: Data are available upon request.

Conflicts of Interest: The authors declare no conflicts of interest.

References

1. Alam, A.M.; Subhan, N.; Rahman, M.M.; Uddin, S.J.; Reza, H.M.; Sarker, S.D. Effect of citrus flavonoids, naringin and naringenin, on metabolic syndrome and their mechanisms of action. *Adv. Nutr.* **2014**, *5*, 404–417. [CrossRef] [PubMed]
2. Fresh Fruit Portal. Citrus Exports: Soft Citrus to Drive Export Growth in 2020–21. Available online: https://www.freshfruitportal.com/news/2021/07/23/soft-citrus-drives-growth-in-global-citrus-exports-in-2020-21/ (accessed on 23 July 2024).
3. Palou, L. Penicillium digitatum, *Penicillium italicum* (green mold, blue mold). In *Postharvest Decay*; Bau-tista-Baños, S., Ed.; Academic Press: Cambridge, MA, USA, 2014; pp. 45–102. [CrossRef]
4. Guyomard, H.; Soler, L.G.; Détang-Dessendre, C.; Réquillart, V. The European Green Deal improves the sustainability of food systems but has uneven economic impacts on consumers and farmers. Com-mun. *Earth Environ.* **2023**, *4*, 358. [CrossRef]
5. Hernández-Carrillo, J.G.; Orta-Zavalza, E.; González-Rodríguez, S.E.; Montoya-Torres, C.; Sepúlve-da-Ahumada, D.R.; Ortiz-rivera, Y. Evaluation of the effectivity of reuterin in pectin edible coatings to extend the shelf-life of strawberries during cold storage. *Food Packag. Shelf Life* **2021**, *30*, 100760. [CrossRef]
6. Heras, M.; Huang, C.C.; Chang, C.W.; Lu, K.H. Trends in chitosan-based films and coatings: A systematic review of the incorporated biopreservatives, biological properties, and nanotechnology applications in meat preservation. *Food Packag. Shelf Life* **2024**, *42*, 101259. [CrossRef]
7. Triunfo, M.; Tafi, E.; Guarnieri, A.; Salvia, R.; Scieuzo, C.; Hahn, T.; Zibek, S.; Gagliardini, A.; Panariello, L.; Coltelli, M.B. Characterization of chitin and chitosan derived from *Hermetia illucens*, a further step in a circular economy process. *Sci. Rep.* **2022**, *12*, 6613. [CrossRef] [PubMed]
8. Kou, S.; Peters, L.M.; Mucalo, M.R. Chitosan: A review of sources and preparation methods. *Int. J. Biol. Macromol.* **2021**, *169*, 85–94. [CrossRef] [PubMed]
9. Bill, M.; Sivakumar, D.; Korsten, L.; Thompson, A.K. The efficacy of combined application of edible coat-ings and thyme oil in inducing resistance components in avocado (*Persea americana* Mill.) against anthrac-nose during post-harvest storage. *Crop Prot.* **2014**, *64*, 159–167. [CrossRef]
10. Chien, P.J.; Sheu, F.; Lin, H. Coating citrus (*Murcott tangor*) fruit with low molecular weight chitosan increases postharvest quality and shelf life. *Food Chem.* **2007**, *100*, 1160–1164. [CrossRef]
11. Perdones, A.; Escriche, I.; Chiralt, A.; Vargas, M. Effect of chitosan–lemon essential oil coatings on volatile profile of strawberries during storage. *Food Chem.* **2016**, *197 Pt A*, 979–986. [CrossRef]
12. Sánchez-González, L.; Cháfer, M.; Chiralt, A.; González-Martínez, C. Physical properties of edible chitosan films containing bergamot essential oil and their inhibitory action on *Penicillium italicum*. *Carbohydr. Polym.* **2010**, *82*, 277–283. [CrossRef]

13. Elsabagh, R.; Ibrahim, S.S.; Abd-Elaaty, E.M.; Abdeen, A.; Rayan, A.M.; Ibrahim, S.F.; Morsy, M.K. Chitosan edible coating: A potential control of toxic biogenic amines and enhancing the quality and shelf life of chilled tuna filets. *Front. Sustain. Food Syst.* **2023**, *7*, 1177010. [CrossRef]
14. Phala, K.; Mapossa, A.B.; Augustyn, W.; Combrinck, S.; Botha, B. Development of EVA and LLDPE polymer-based carvone and spearmint essential oil release systems for citrus postharvest diseases applications. *Arab. J. Chem.* **2023**, *16*, 104458. [CrossRef]
15. Komaiko, J.; Mcclements, D.J. Low-energy formation of edible nanoemulsion by spontaneous emulsification: Factors influencing particle size. *J. Food Eng.* **2015**, *146*, 122–128. [CrossRef]
16. de Oliveira Filho, J.G.; Miranda, M.; Ferreira, M.D.; Plotto, A. Nanoemulsions as edible coatings: A potential strategy for fresh fruits and vegetables preservation. *Foods* **2021**, *10*, 2438. [CrossRef] [PubMed]
17. Mushtaq, A.; Wani, S.M.; Malik, A.R.; Gull, A.; Ramniwas, S.; Nayik, G.A.; Ercisli, S.; Marc, R.A.; Ullah, R.; Bari, A. Recent insights into anoemulsions: Their preparation, properties and applications. *Food Chem. X* **2023**, *18*, 100684. [CrossRef] [PubMed]
18. Badawy, M.E.I.; Rabea, E.I. A biopolymer chitosan and its derivatives as promising antimicrobial agents against plant pathogens and their applications in crop protection. *Int. J. Carbohydr. Chem.* **2011**, *2011*, 460381. [CrossRef]
19. Arendrup, M.C.; Kahlmeter, G.; Guinea, J.; Meletiadis, J. How to: Perform antifungal susceptibility testing of microconidia-forming dermatophytes following the new reference EUCAST method E.Def 11.0, exemplified by Trichophyton. *Clin. Microbiol. Infect.* **2021**, *27*, 55–60. [CrossRef]
20. Sellamuthu, P.S.; Sivakumar, D.; Soundy, P. Antifungal activity and chemical composition of thyme, peppermint and citronella oils in vapor phase against avocado and peach postharvest pathogens. *J. Food Saf.* **2013**, *33*, 86–93. [CrossRef]
21. Sivakumar, D.; Wijeratnam, R.W.; Wijesundera, R.L.C. Effect of GRAS compounds on mycelial growth, pectic enzyme activity and disease severity of postharvest pathogens on Rambutan (*Nephelium lappaceum*). *Phytoparasitica* **2001**, *29*, 135–141. [CrossRef]
22. Malfatti, A.D.R.; Mallmann, G.C.; Filho, L.C.O.; Carniel, L.S.C.; Cruz, S.P.; Klauberg-Filho, O. Ecotoxicological test to assess effects of herbicides on spore germination of *Rhizophagus clarus* and *Gigaspora albida*. *Ecotoxicol. Environ. Saf.* **2021**, *27*, 55–60. [CrossRef] [PubMed]
23. Galus, S.; Kadzińska, J. Whey protein edible films modified with almond and walnut oils. *Food Hydrocoll.* **2016**, *52*, 78–86. [CrossRef]
24. Das, S.; Chaudhari, A.K.; Singh, V.K.; Dwivedy, A.K.; Dubey, N.K. Chitosan based encapsulation of *Valeriana officinalis* essential oil as edible coating for inhibition of fungi and aflatoxin B1 contamination, nutritional quality improvement, and shelf-life extension of *Citrus sinensis* fruits. *Int. J. Biol. Macromol.* **2023**, *233*, 123565. [CrossRef] [PubMed]
25. Sun, L.; Sun, J.; Chen, L.; Niu, P.; Yang, X.; Guo, Y. Preparation and characterization of chitosan film incor-porated with thinned young apple polyphenols as an active packaging material. *Carbohydr. Polym.* **2017**, *163*, 81–91. [CrossRef]
26. Elshamy, S.; Khadizatul, K.; Uemura, K. Chitosan-based film incorporated with essential oil nanoemulsion foreseeing enhanced antimicrobial effect. *J. Food Sci. Technol.* **2021**, *58*, 3314–3327. [CrossRef]
27. Rui, L.; Li, Y.; Wu, X.; Wang, Y.; Xia, X. Effect of clove essential oil nanoemulsion on physicochemical and antioxidant properties of chitosan film. *Int. J. Biol. Macromol.* **2024**, *263*, 130286. [CrossRef]
28. Pillai, S.K.; Maubane, L.; Sinha Ray, S.; Khumalo, V.; Bill, M.; Sivakumar, D. Development of antifungal films based on low-density polyethylene and thyme oil for avocado packaging. *J. Appl. Polym. Sci.* **2016**, *133*, 8. [CrossRef]
29. Pillai, S.K.; Ray, S.S. Inorganic-organic hybrid polymers for food packaging. In *Functional Polymers in Food Science: From Technology to Biology*; Wiley: New York, NY, USA, 2015; pp. 281–322. [CrossRef]
30. Osset-Trénor, P.; Pascual-Ahuir, A.; Proft, M. Fungal Drug response and antimicrobial resistance. *J. Fungi* **2023**, *9*, 565. [CrossRef] [PubMed]
31. Zulu, L.; Gao, H.; Zhu, Y.; Wu, H.; Xie, Y.; Liu, X.; Yao, H.; Rao, Q. Antifungal effects of seven plant essential oils against *Penicillium digitatum*. *Chem. Biol. Technol. Agric.* **2023**, *10*, 82. [CrossRef]
32. Szczerbanik, M.; Jobling, J.J.; Morris, S.; Holford, P. Essential oil vapours control some common posthar-vest fungal pathogens. *Aust. J. Exp. Agric.* **2007**, *47*, 103–109. [CrossRef]
33. Yahyazadeh, M.; Omidbaigi, R.; Zare, R.; Taheri, H. Effect of some essential oils on mycelial growth of Pen-icillium digitatum Sacc. *World J. Microbiol. Biotechnol.* **2008**, *24*, 1445–1450. [CrossRef]
34. Tao, N.; Jia, L.; Zhou, H. Anti-fungal activity of *Citrus reticulata Blanco* essential oil against *Penicillium italicum* and *Penicillium digitatum*. *Food Chem.* **2014**, *153*, 265–271. [CrossRef] [PubMed]
35. Pârvu, M.; Pârvu, A.E.; Crăciun, C.; Barbu-Tudoran, L.; Tămaş, M. Antifungal activities of *Chelidonium majus* extract on *Botrytis cinerea in vitro* and ultrastructural changes in its conidia. *J. Phytopathol.* **2008**, *156*, 550–552. [CrossRef]
36. Aswathanarayan, J.B.; Vittal, R.R. Nanoemulsions and their potential applications in food industry. *Front. Sustain. Food Syst.* **2019**, *3*, 95. [CrossRef]
37. de la Cruz, A.S.L.; Barrera-Cortés, J.; Lina-García, L.P.; Ramos-Valdivia, A.C.; Santillán, R. Nanoemulsified formulation of *Cedrela odorata* essential oil and its larvicidal effect against *Spodoptera frugiperda* (J.E. Smith). *Molecules* **2022**, *27*, 2975. [CrossRef] [PubMed]

38. Tariq, H.; Rehman, A.; Kishwar, F.; Raza, Z.A. Citric acid cross-linking of chitosan encapsulated spearmint oil for antibacterial cellulosic fabric. *Polym. Sci. Ser. A* **2022**, *64*, 456–466. [CrossRef] [PubMed]
39. Yousefi, M.; Khanniri, E.; Sohrabvandi, S.; Khorshidian, N.; Mortazavian, A.M. Encapsulation of *Heracleum persicum* essential oil in chitosan nanoparticles and its application in yogurt. *Front. Nutr.* **2023**, *10*, 1130425. [CrossRef] [PubMed]
40. Essid, R.; Ayed, A.; Djebali, K.; Saad, H.; Srasra, M.; Othmani, Y.; Fares, N.; Jallouli, S.; Abid, I.; Alothman, M.R. Anti-candida and anti-leishmanial activities of encapsulated *Cinnamomum verum* essential oil in chitosan nanoparticles. *Molecules* **2023**, *28*, 5681. [CrossRef] [PubMed]
41. Bonilla, J.; Atarés, L.; Vargas, M.; Chiralt, A. Effect of basil and thyme essential oils and homogenization conditions on properties of chitosan-based films. *Food Hydrocoll.* **2012**, *26*, 9–16. [CrossRef]
42. Hong, F.; Qiu, P.; Wang, Y.; Ren, P.; Liu, J.; Zhao, J.; Gou, D. Chitosan-based hydrogels: From preparation to applications, a review. *Food Chem. X* **2024**, *21*, 101095. [CrossRef]
43. de Oliveira Filho, J.G.; de Deus, I.P.B.; Valadares, A.C.F.; Fernandes, C.C.; Estevam, E.B.B.; Egea, M.B. Chitosan film with *Citrus limonia* essential oil: Physical and morphological properties and antibacterial activity. *Colloids Interfaces* **2020**, *4*, 18. [CrossRef]
44. Haghighi, H.; Biard, S.; Bigi, F.; De Leo, R.; Bedin, E.; Pfeifer, F.; Siesler, H.W.; Licciardello, F.; Pulvirenti, A. Comprehensive characterization of active chitosan-gelatin blend films enriched with different essential oils. *Food Hydrocoll.* **2019**, *95*, 33–42. [CrossRef]
45. Croll, S.G. Stress and embrittlement in organic coatings during general weathering exposure: A review. *Prog. Org. Coat.* **2022**, *172*, 107085. [CrossRef]
46. Silva, M.I.; Malitckii, E.; Santos, T.G.; Vilaça, P. Review of conventional and advanced non-destructive testing techniques for detection and characterization of small-scale defects. *Prog. Mater. Sci.* **2023**, *138*, 101155. [CrossRef]
47. Zhang, X.; Liu, D.; Jin, T.Z.; Chen, W.; He, Q.; Zou, Z.; Guo, M. Preparation and characterization of gellan gum-chitosan polyelectrolyte complex films with the incorporation of thyme essential oil nanoemulsion. *Food Hydrocoll.* **2021**, *114*, 106570. [CrossRef]
48. Lee, J.S.; Lee, E.; Han, J. Enhancement of the water-resistance properties of an edible film prepared from mung bean starch via the incorporation of sunflower seed oil. *Sci. Rep.* **2020**, *10*, 13622. [CrossRef] [PubMed]
49. Gorjian, H.; Mihankhah, P.; Khaligh, N.G. Influence of tween nature and type on physicochemical proper-ties and stability of spearmint essential oil (*Mentha spicata* L.) stabilized with basil seed mucilage nanoemulsion. *J. Mol. Liq.* **2022**, *359*, 119379. [CrossRef]
50. Nazari, M.; Majdi, H.; Gholizadeh, P.; Kafil, H.S.; Hamishehkar, H.; Zarchi, A.A.K.; Khoddami, A. An eco-friendly chitosan/cellulose acetate hybrid nanostructure containing *Ziziphora clinopodioides* essential oils for active food packaging applications. *Int. J. Biol. Macromol.* **2023**, *235*, 123885. [CrossRef] [PubMed]
51. Zhao, Y.; Zhang, Y.; Dong, H.; Wu, W.; Yang, X.; He, Q. Functional biopolymers for food packaging: Formation mechanism and performance improvement of chitosan-based composites. *Food Biosci.* **2023**, 102927. [CrossRef]
52. Al-Harrasi, A.; Bhtaia, S.; Al-Azri, M.S.; Makeen, H.A.; Albratty, M.; Alhazmi, H.A.; Behl, T. Development and characterization of chitosan and porphyran based composite edible films containing ginger essential oil. *Polymers* **2022**, *14*, 1782. [CrossRef] [PubMed]
53. Mao, S.; Ren, Y.; Wei, C.; Chen, S.; Ye, X.; Jinhu, T. Development of novel EGCG/Fe loaded sodium alginate-based packaging films with antibacterial and slow-release properties. *Food Hydrocoll.* **2023**, *145*, 109032. [CrossRef]
54. Liu, Y.; Liu, R.; Shi, J.; Zhang, R.; Tang, H.; Xie, C.; Jiang, L. Chitosan/esterified chitin nanofibers nanocom-posite films incorporated with rose essential oil: Structure, physicochemical characterization, antioxidant and antibacterial properties. *Food Chem. X* **2023**, *18*, 100714. [CrossRef] [PubMed]
55. du Plooy, W.; Regnier, T.; Combrinck, S. Essential oil amended coatings as alternatives to synthetic fungi-cides in citrus postharvest management. *Postharvest Biol Technol.* **2009**, *53*, 117–122. [CrossRef]